DOI 10.24425/aee.2025.153903

Initial conditions for a transient steady-state induction machine simulation based on time-harmonic and multi-harmonic solutions

TOMASZ GARBIEC

Opole University of Technology, Faculty of Electrical Engineering, Automatic Control and Informatics
45-758 Opole, ul. Prószkowska 76

e-mail: ✉ *t.garbiec@po.edu.pl*

(Received: 29.08.2024, revised: 17.04.2025)

Abstract: The paper presents the results of the author's research on effectively determining the initial conditions for the time-stepping model of a high-speed inverter-driven induction machine. The classical time-harmonic and multi-harmonic models based on the multidimensional effective magnetic permeability were used and compared as a preconditioner for the time-stepping model to speed up the steady-state solution. The carried-out simulation experiment proved that using both approaches radically accelerates computations. Furthermore, it has been shown that the multi-harmonic model is much more effective for problems with strong harmonic effects.

Key words: effective magnetic permeability, finite element method, harmonic model, induction machines, steady-state solution

1. Introduction

The finite element method is indispensable for designing and analysing all electrical machines. Most professional computational packages based on this method enable analysis in three ways, namely as a magnetostatic problem, a time-harmonic (TH) problem, or a time-domain problem (time-stepping model) [1]. Concerning induction machines, the latter two approaches are mainly used in practice. As confirmed in the 1980s [2], the time-harmonic model is very effective for preliminary calculations because of its short execution time. Unfortunately, with this approach, it is impossible to accurately account for the influence of higher harmonics (due to nonsinusoidal

supplying voltages and slotting) and some effects related to magnetic saturation or rotor movement. Sometimes, especially when detailed loss analysis is needed, it may lead to unacceptable calculation errors [3, 4]. For such cases, finite-element time-stepping models offer much better accuracy. However, the problem is still the significant computational cost associated with the influence of eddy currents in the rotor and large electromagnetic time constants [5, 6]. It justifies the search for methods of accelerating computations, especially when only the steady-state solution is required [6].

Methods to accelerate the calculation of steady-state solutions using the time-stepping models can be divided into three main groups. The first involves hardware acceleration using parallel and distributed computing [7], now available in many professional electromagnetic calculation packages like Altair Flux, ANSYS Maxwell and JMAG. The second group involves special computational and implementation techniques, such as using a Shooting-Newton/GMRES Approach [8] or the methods shown in the papers [9–12], where time-periodicity conditions were introduced. However, some of these methods have limited applicability concerning induction machines because there is no fundamental relationship between the rotor angular velocity and frequency of the supplying waveforms [8]. The third group involves special modifications of the initial conditions for solving the time-stepping model or supplying conditions at the initial stage of computations (relaxation of sources). Very interesting examples of such approaches are presented in [6, 13, 14]. In [6], the Authors used additional current sources (currents calculated using the TH model), which were added at the initial stage of simulation to the time-stepping field-circuit model and solved with the rotor locked. According to the Authors, this approach can reduce the calculation time by up to 34% compared to the solution with zero initial conditions. In [13], the Authors presented a hybrid simulation approach coupling numerical (static FE model) and analytical methods to reduce computation time for simulation of the torque-speed operating points, whereas in [14], the TH model was used for calculating the initial conditions for the time-stepping model.

Of the methods mentioned above, the last one (using a TH model for determining the initial conditions) deserves special attention because of its simplicity (compared to the other methods) and the fact that there is no need to modify the base time-stepping model. This approach shows great potential for application in commercial and in-house software. It encourages the author to extend its main idea on problems with strong harmonic effects and use a multi-harmonic (MH) field-circuit model [4] (instead of the classical TH approach) as a preconditioner for the time-stepping model. The MH model accounts for nonsinusoidal supplying waveforms and slotting effects [4]. However, the complexity of its implementation is much higher than that of the TH model. To the best of the author's knowledge, utilising the field-circuit MH model for the determination of the initial condition for the time-stepping model has not been presented in the literature, so to validate its practical usefulness and compare it with the TH model, a computational experiment has been carried out.

2. Computational experiment

The computational experiment involved determining the initial conditions using both the MH and TH models for an experimental high-speed, low-power induction machine fed from a quasi-square voltage inverter (Fig. 1, Table 1). For the analysed case, higher time-harmonics and permeance harmonics strongly influence motor performance, especially the solid rotor losses [15, 16]. The calculations were carried out by taking as the excitation fragments of the

supplying voltage waveform recorded during measurements (Table 2, Fig. 2). For the considered machine, the field-circuit two-dimensional time-stepping model was implemented in the Matlab®/Octave scripting language (the GMSH software package was used as the mesh generator [17]) and validated (Fig. 2(b)). Rotor movement was modelled using the moving-band technique and the rotor-end effects were considered using the so-called effective σ_{eff} calculated numerically.

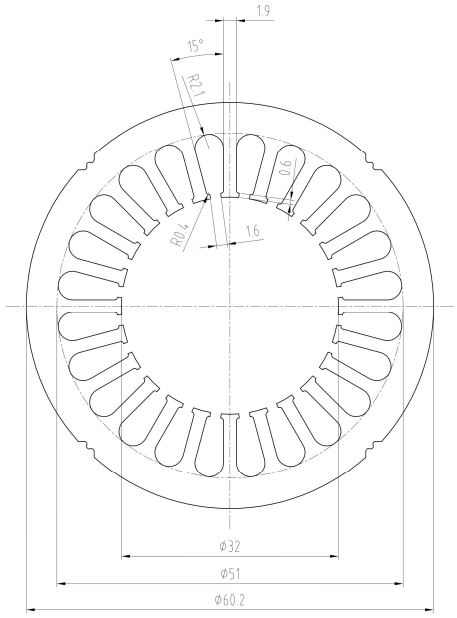

(a)

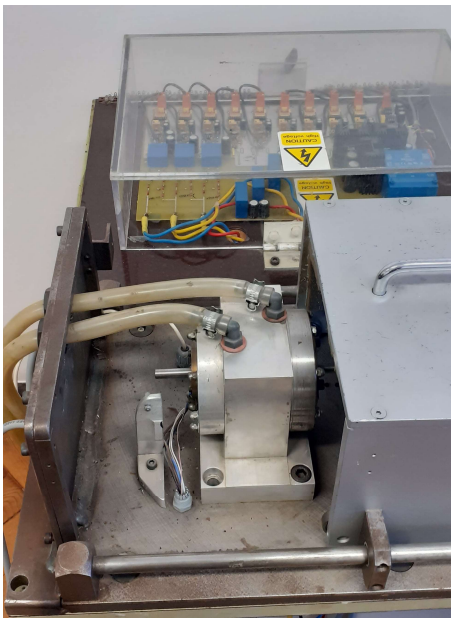

(b)

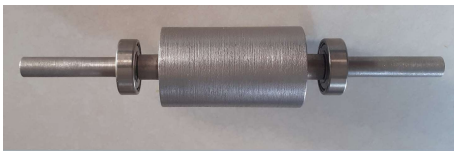

(c)

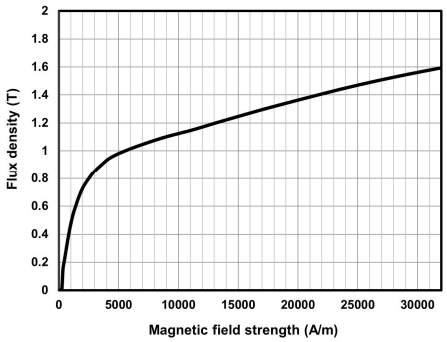

(d)

Fig. 1. Analysed machine: dimension of the stator package (a); experimental set-up (b); uniform solid rotor (c); measured BH curve for the rotor material (d)

Table 1. Basic specifications of the experimental solid-rotor induction motor

Number of pole-pairs	2
Number of stator slots	24
Stator package material	M270-35A
Winding type	Two-layer, fully-pitched
Number of turns per slot	18
Stator length Stator bore diameter Air-gap length Rotor length	32 mm 32 mm 0.25 mm 54 mm
Rotor material	Mild steel
Rotor material conductivity at 20°C	3.55 MS/m

Table 2. Main conditions under the test

Rotational speed range	5 kRPM–14 kRPM
Fundamental slip values	66.66%–6.66%
Supplying converter type	Quasi-square voltage inverter
Fundamental frequency	496 Hz
DC-bus voltage	100 V

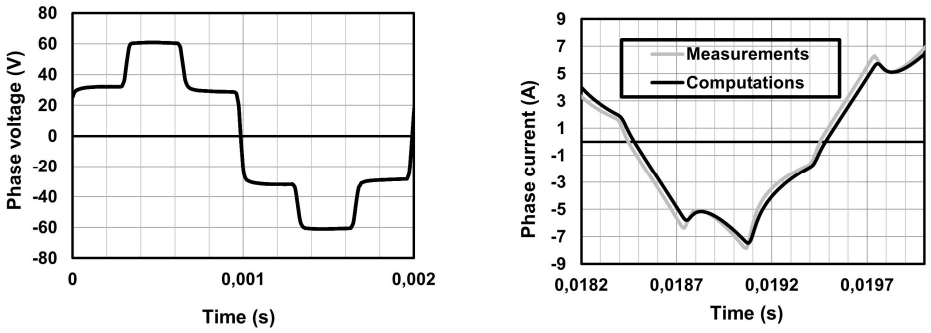

(a) (b)

Fig. 2. Measured waveforms: supplying phase voltage used in computations (a); phase current at 10 000 RPM (b)

3. Determining the initial conditions

3.1. Time-harmonic field-circuit model used as the preconditioner

For the considered example, it was assumed that the excitation for the TH model is the pure sine voltage of the complex amplitude equal to the complex amplitude of the fundamental harmonic derived from FFT analysis of the measured waveforms. The system of equations for the model takes the form:

$$\begin{bmatrix} \boldsymbol{S}(\mu_{\text{eff1}}) + \text{j}\omega_1 s_1 \boldsymbol{G} & -\boldsymbol{D}^T \boldsymbol{K}^T \\ \text{j}\omega_1 l_z \boldsymbol{K}\boldsymbol{D} & \boldsymbol{K}\underline{\boldsymbol{Z}}\boldsymbol{K}^T \end{bmatrix} \begin{bmatrix} \boldsymbol{\varphi} \\ \underline{\boldsymbol{I}} \end{bmatrix} = \begin{bmatrix} \boldsymbol{0} \\ \boldsymbol{K}\underline{\boldsymbol{E}} \end{bmatrix}, \tag{1}$$

where $\boldsymbol{S}$ is the reluctivity matrix, $\text{j} = \sqrt{-1}$, ω_1 and s_1 are the fundamental pulsation and slip, respectively, $\boldsymbol{G}$ is the conductivity matrix, $\boldsymbol{D}$ is the matrix attributed to the winding function, $\boldsymbol{K}$ is the loop incidence matrix, l_z is stator package length, $\underline{\boldsymbol{Z}}$ is the stator impedance matrix, $\underline{\boldsymbol{\varphi}}$ is the vector of nodal values of the complex magnetic vector potential, $\underline{\boldsymbol{I}}$ is the vector of the complex stator loop currents, $\underline{\boldsymbol{E}}$ is the vector of the complex magnitudes of the supplying voltages and μ_{eff1} is the effective magnetic permeability calculated as:

$$\mu_{\text{eff1}}(H_1) = \frac{2}{\pi H_1} \int_0^{\pi} \mu_{\text{DC}}(H_1 \sin\alpha) H_1 \sin^2\alpha d\alpha, \tag{2}$$

where μ_{DC} is the DC magnetic permeability and H_1 is the amplitude of the magnetic field strength. Next, the initial conditions vector for the time-stepping model can be expressed as [14]:

$$\begin{bmatrix} \boldsymbol{\varphi} \\ \boldsymbol{I} \end{bmatrix}_{\boldsymbol{0}} = \text{Re}\left(\begin{bmatrix} \underline{\boldsymbol{\varphi}} \\ \underline{\boldsymbol{I}} \end{bmatrix} \right). \tag{3}$$

3.2. Multi-harmonic field-circuit model used as the preconditioner

The multi-harmonic model used in this work as the second method to determine the initial conditions for the time-stepping model was presented in detail in [3,4,18]. As shown, this approach is much more accurate than the TH model when the analysed problem involves a strong influence of higher harmonics.

First, the FFT on the nonsinusoidal supplying voltage waveform was performed to create the MH model. Then, the complex amplitudes of the N selected harmonics were extracted (here 1st, 5th, 7th, 11th, and 13th harmonics were considered) and used as the excitation for N MH field-circuit sub-models (each sub-model with strong coupling between the stator model and K rotors models associated with the K considered permeance harmonics (Fig. 3) [3, 18]).

Each sub-model was excited by the corresponding harmonic of the supply voltage, considering its frequency, phase and the associated slip value corresponding to the rotor speed. The individual sub-models were solved independently (possible parallelization), assuming in a given iterative step a constant distribution of the "frozen" multidimensional effective magnetic permeability, which

after each iteration of the algorithm (the fixed-point method) was updated based on the formula [4]:

$$\mu_{\text{eff}}(H_1, ..., H_n) = \frac{\sqrt{B_1^2 + ... + B_n^2}}{\sqrt{H_1^2 + ... + H_n^2}}, \tag{4}$$

where:

$$B_n = \frac{2}{\pi} \int_0^{\pi} \mu_{\text{DC}} (H_1 \sin 1\alpha + \ldots + H_n \sin n\alpha)(H_1 \sin 1\alpha + \ldots + H_n \sin n\alpha) \sin n\alpha d\alpha \tag{5}$$

is the amplitude of the magnetic flux density associated with the n-th harmonic of the supplying voltage and H_n is the amplitude of the magnetic field strength associated with the n-th harmonic of the supplying voltage. The multidimensional effective permeability expressed as (4) is calculated based on the assumption of sinusoidal variation of the magnetic field strength. When only the fundamental harmonic is considered (4) reduces to (2).

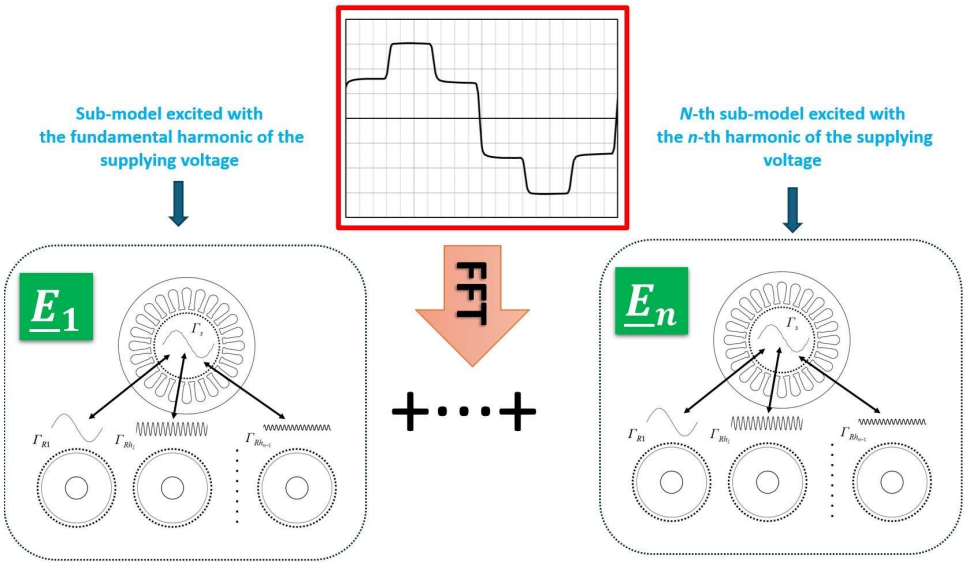

Fig. 3. The main idea of the multi-harmonic model used for the initial conditions calculations (weak coupling between N strongly-coupled sub-models comprising of the stator model and K rotor models associated with K permeance harmonics)

The system of equations, coupling the stator and rotors in the particular sub-models via indefinite Lagrange multipliers for the n-th sub-model, is expressed as:

$$\begin{bmatrix} \boldsymbol{M}_{11n}(\mu_{\text{eff}}) & \boldsymbol{M}_{12n} & \boldsymbol{M}_{13} \\ \boldsymbol{M}_{21n} & \boldsymbol{M}_{22n} & \boldsymbol{0} \\ \boldsymbol{M}_{31} & \boldsymbol{0} & \boldsymbol{0} \end{bmatrix} \begin{bmatrix} \underline{\boldsymbol{\varphi}}_n \\ \underline{\boldsymbol{I}}_n \\ \underline{\boldsymbol{\lambda}}_n \end{bmatrix} = \begin{bmatrix} \boldsymbol{0} \\ \boldsymbol{K}\underline{\boldsymbol{E}}_n \\ \boldsymbol{0} \end{bmatrix}, \tag{6}$$

where:

$$\boldsymbol{M}_{\mathbf{11}n} = \begin{bmatrix} \boldsymbol{S}_S(\mu_{\text{eff}}) & \mathbf{0} & \mathbf{0} & \vdots & \mathbf{0} \\ \mathbf{0} & \boldsymbol{S}_R(\mu_{\text{eff}}) + \mathrm{j}s_{n1}\omega_n\boldsymbol{G}_R & \mathbf{0} & \vdots & \mathbf{0} \\ \mathbf{0} & \mathbf{0} & \ddots & \vdots & \mathbf{0} \\ \cdots & \cdots & \cdots & \ddots & \cdots \\ \mathbf{0} & \mathbf{0} & \mathbf{0} & \cdots & \boldsymbol{S}_R(\mu_{\text{eff}}) + \mathrm{j}s_{nh}\omega_n\boldsymbol{G}_R \end{bmatrix}, \tag{7}$$

$$\boldsymbol{M}_{12n} = -\boldsymbol{M}_{21n}^T/(\mathrm{j}\omega_n l_z) = \left[-\boldsymbol{D}^T\boldsymbol{K}^T \; \mathbf{0} \; \mathbf{0} \cdots \mathbf{0} \right]^{\boldsymbol{T}}, \tag{8}$$

$$\boldsymbol{M}_{\mathbf{13}} = \boldsymbol{M}_{\mathbf{31}}^T = \begin{bmatrix} -\underline{\boldsymbol{Q}}_s^T & -\underline{\boldsymbol{Q}}_s^T\boldsymbol{F}_1^*\boldsymbol{F}_1 & \cdots & -\underline{\boldsymbol{Q}}_s^T\boldsymbol{F}_h^*\boldsymbol{F}_h \\ \boldsymbol{Q}_R^T & \mathbf{0} & \cdots & \mathbf{0} \\ \mathbf{0} & \boldsymbol{Q}_R^T & \cdots & \mathbf{0} \\ \cdots & \cdots & \cdots & \cdots \\ \mathbf{0} & \mathbf{0} & \cdots & \mathbf{Q}_R^T \end{bmatrix}, \tag{9}$$

$$\boldsymbol{M}_{\mathbf{22}n} = \boldsymbol{K}\underline{\boldsymbol{Z}}_n\boldsymbol{K}^T, \tag{10}$$

and $\boldsymbol{S}_S$, $\boldsymbol{S}_R$ are the reluctivity matrices related to the stator and rotors domains, respectively, $\boldsymbol{G}_R$ is the conductivity matrix for the rotor domain, s_{nh} is the slip value for the rotor model associated with n-th time harmonic and h-th permeance harmonic, ω_n is the pulsation of n-th time harmonic, $\underline{\boldsymbol{\varphi}}_n$ is the vector of nodal values of the complex magnetic vector potential, $\underline{\boldsymbol{I}}_n$ is the vector of the complex magnitudes of the stator loop currents, $\underline{\boldsymbol{\lambda}}_n$ is the vector of indefinite complex Lagrange multipliers, $\underline{\boldsymbol{Z}}_n$ is the stator winding impedance matrix, $\boldsymbol{F}_h$, $\boldsymbol{F}_h^*$, are Fourier and Inverse Fourier transform operating matrices allowing propagation of h-th permeance harmonic only and $\boldsymbol{Q}_S$, $\boldsymbol{Q}_R$ are the matrices to pair nodes at interface boundary [3].

As a result of the convergence of the algorithm for solving a nonlinear problem N vectors of solutions (6) are obtained. Next, the initial condition vector for the time-stepping model can be expressed as:

$$\begin{bmatrix} \boldsymbol{\varphi} \\ \boldsymbol{I} \end{bmatrix}_{\mathbf{0}} = \sum_{i=1,..,n} \begin{bmatrix} \left|\underline{\boldsymbol{\varphi}}_i\right| \cos\left(i\omega_1 T + \arg\left(\underline{\boldsymbol{\varphi}}_i\right)\right) \\ \left|\underline{\boldsymbol{I}}_i\right| \cos\left(i\omega_1 T + \arg\left(\underline{\boldsymbol{I}}_i\right)\right) \end{bmatrix}. \tag{11}$$

4. Results of computations

First, the basic performance characteristics of the machine (RMS phase current and torque versus speed) were obtained using different models (the classical time-stepping model, the TH model only and the MH model only, accordingly). For the time-stepping model to quantitatively compare the results obtained, it is necessary to introduce an unambiguous error criterion for obtaining the steady-state. In the present study, the following conditions were used:

$$|i(t) - i(t-T)| < 0.01 \text{ A} \;\wedge\; |m_e(t) - m_e(t-T)| < 0.0001 \text{ Nm}, \tag{12}$$

where: T is the period of the supplying voltage, $i(t)$ is the instantaneous phase current, $m_e(t)$ is the instantaneous electromagnetic torque. A time step Δt for solving the time-stepping model was

set as $\Delta t = T/300$. The comparison of the performance characteristics calculated using different approaches is depicted in Fig. 4. As can be seen only the time-stepping model allows obtaining good enough results, however, accuracy of the MH model is slightly greater than the classical TH model. It is because of the high influence of the higher harmonics in the analysed case.

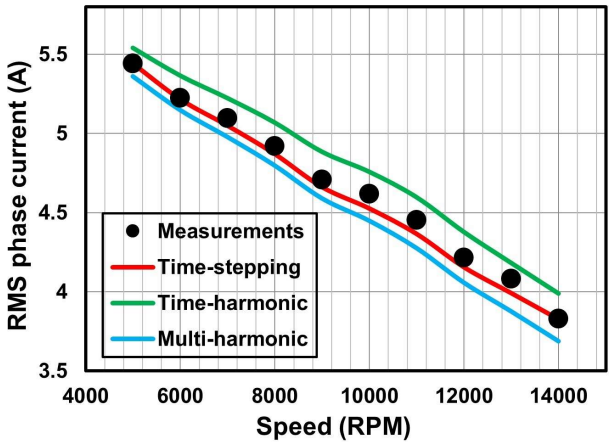

(a)

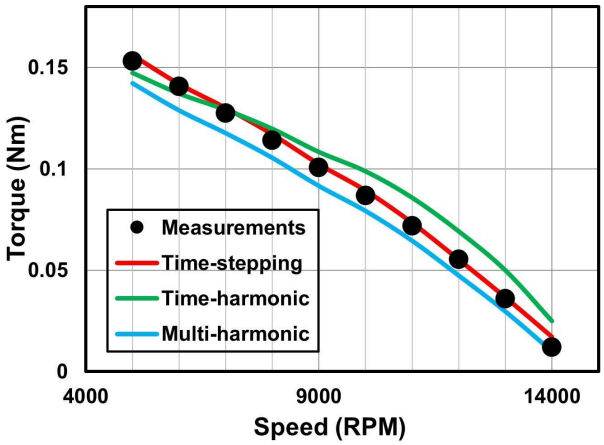

(b)

Fig. 4. Comparison of the results of calculations of the basic operational characteristics using different appraoches: RMS phase current versus speed (a); electromagnetic torque versus speed (b)

The next step involved using the TH and MH models as the preconditioners for calculating the initial conditions according to (3) and (11), respectively. For all calculations, the steady-state was obtained when (12) was true. Because the time of calculations depends strongly on the performance of a workstation used, in this paper, to assess both preconditioners, the number of

time steps needed to obtain the steady state was used instead of the total execution time. Results of the comparison of the results of computations using the time-stepping model with the different initial conditions are presented in Figs. 5– 6 and Table 3.

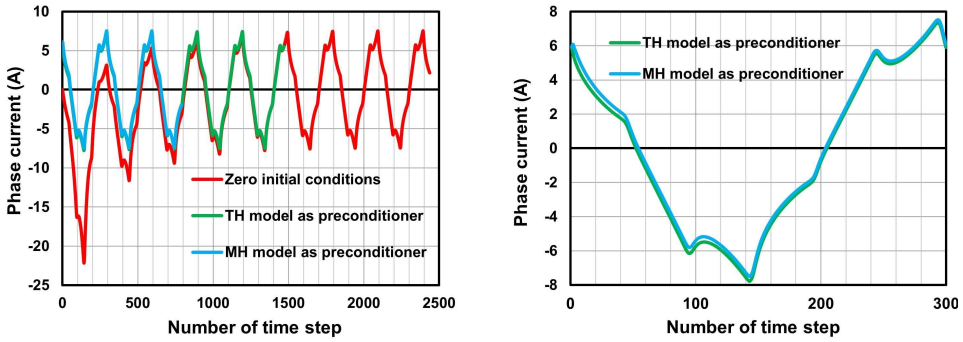

(a) (b)

Fig. 5. Comparison of the results of calculations of the phase current waveform using different initial conditions for a speed equal to 10 000 RPM: the whole waveforms computed until the steady-state condition is true (a); initial fragments of the computed waveforms (b)

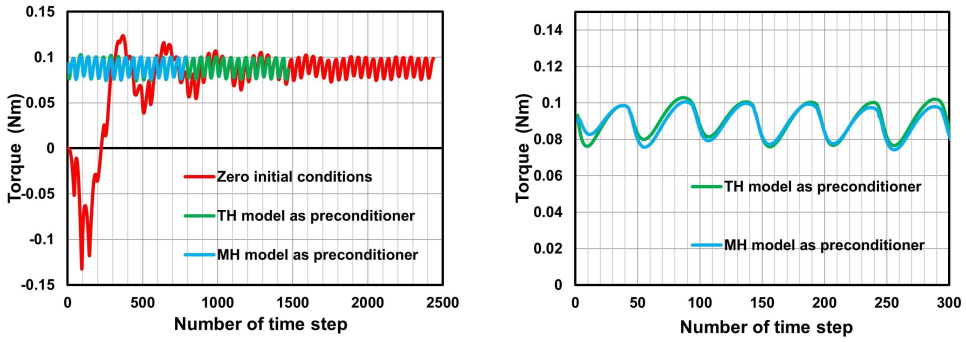

(a) (b)

Fig. 6. Comparison of the results of calculations of the electromagnetic torque waveform using different initial conditions for a speed equal to 10 000 RPM: the whole waveforms computed until the steady-state condition is true (a); initial fragments of the computed waveforms (b)

As can be seen, using both preconditioners makes it possible to significantly reduce the number of time steps needed to obtain the steady-state, however, the MH model used as the preconditioner is much more effective. It justifies its usage despite the extensively higher complexity of its implementation and the much longer time needed to calculate initial conditions (see Table 4). The reduction in calculation time and the difference between the initial conditions computed using the two different models should increase with increasing transient time and the influence

of higher harmonics. To confirm this hypothesis, further calculations were performed for a slip equal to the base case at 10 000 rpm, but with the five much higher frequency and voltage values increased by a factor of two (see Figs. 7– 8 and Table 5). As can be seen, the MH model used as the preconditioner allows obtaining the steady-state practically after one period of the supplying voltage and reducing computation time to per cent of that one using the zero initial conditions.

Table 3. Number of time steps needed to calculate the steady-state until the condition (12) is true (I – the zero initial conditions, II – the initial conditions obtained using the TH model, III – the initial conditions obtained using the MH model)

Speed (RPM)	**I**	**II**	**III**
5 000	3061	1037	509
6 000	2891	638	841
7 000	2505	1528	795
8 000	2142	1372	345
9 000	2120	1373	342
10 000	2438	1469	790
11 000	2798	888	711
12 000	2435	1194	775
13 000	2885	1477	963
14 000	2870	1378	503

Table 4. Total time of computation for speed equal to 10 000 RPM carried out on the standard PC (AMD Ryzen 5 5600H, 32 GB RAM)

Zero initial conditions	**TH model used as the preconditioner***	**MH model used as the preconditioner***
3 550 s	1 785 s	1 050 s

*Including a preconditioner execution time (5.4 s for the TH model and 108 s for the MH model, respectively).

Table 5. Number of time steps needed to calculate the steady-state until the condition (12) is true at a speed equal to 50 000 RPM with increased frequency (×5) and voltage (×2)

Speed (RPM)	**I**	**II**	**III**
50 000	6 201	959	361

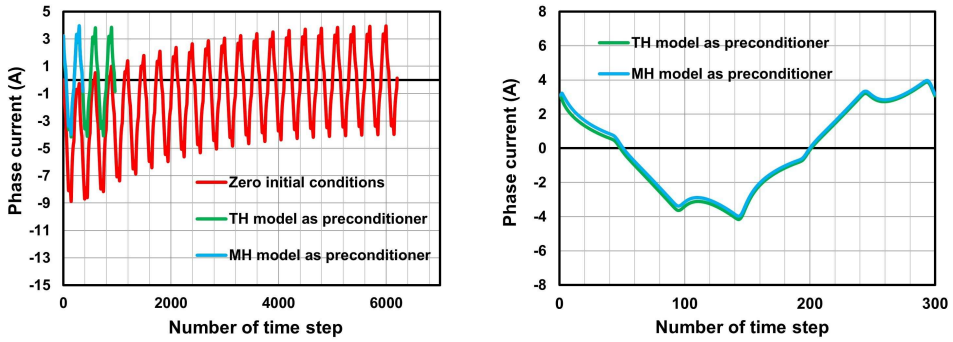

Fig. 7. Comparison of the results of calculations of the phase current waveform using different initial conditions for a speed equal to 50 000 RPM: the whole waveforms computed until the steady-state condition is true (a); initial fragments of the computed waveforms (b)

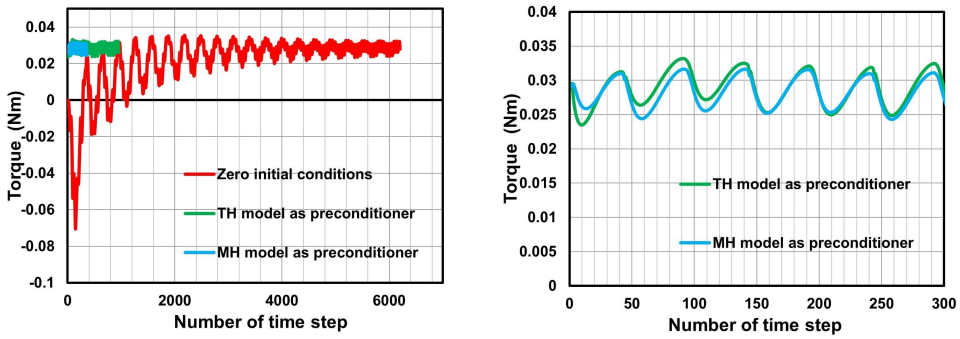

Fig. 8. Comparison of the results of calculations of the electromagnetic torque waveform using different initial conditions for a speed equal to 50 000 RPM: the whole waveforms computed until the steady-state condition is true (a); initial fragments of the computed waveforms (b)

5. Conclusions

The experiment confirmed that for the analysed problem, it is possible to efficiently determine the initial conditions for a time-stepping model and reach the steady-state solution practically after two periods of the supplying voltage. It significantly reduced the computation time to nearly ten per cent of the time required to solve the model with zero initial conditions. Of course, the results shown in the paper apply only to a particular case, so it is necessary to conduct further studies for another types of machines under different operating conditions. The obtained results, together with those one from the author's earlier work, however, allow us to hope that the presented method can prove its usefulness in most cases encountered in practice involving computation of

the steady-states for induction machines using their FEM time-stepping models. The limitation is not the nonsinusoidal supplying voltages or their asymmetry [4]. Furthermore, it was shown that the MH model is more effective than the TH model when the high presence of the higher harmonic is observed. However, further research is needed. So, the next planned step is to develop a model of a squirrel-cage induction machine, taking into account the skew and reduction of the computational area, and carry out an investigation to what extent it is possible to reduce the computation time of a 2.5D time-stepping model using the nonzero initial conditions. Furthermore, it is necessary to compare the effectiveness of the proposed method to the other different methods presented in the literature, especially those involving time-periodicity conditions and different methods with modification of the initial supplying conditions.

References

[1] Bianchi N., *Electrical Machine Analysis Using Finite Elements*, CRC Press (2005).

[2] Arkkio A., *Analysis of induction motor based on the numerical solution of the magnetic field and circuit equations*, PhD Thesis, Helsinki University of Technology, Espoo (1987).

[3] Garbiec T., Jagiela M., Kulik M., *Application of Nonlinear Complex Polyharmonic Finite-Element Models of High-Speed Solid-Rotor Induction Motors*, IEEE Transaction on Magnetics, no. 56, no. 7515304 (2020), DOI: 10.1109/TMAG.2019.2953987.

[4] Garbiec T., Jagiela M., *Accounting for Slot Harmonics and Nonsinusoidal Unbalanced Voltage Supply in High-Speed Solid-Rotor Induction Motor Using Complex Multi-Harmonic Finite Element Analysis*, Energies, vol. 14, no. 5404 (2021), DOI: 10.3390/en14175404.

[5] Nell M., Lenz J., Hamayer K., *Scaling laws for the FE solutions of induction machines*, Archives of Electrical Engineering, vol. 68, no. 3, pp. 667–695 (2019), DOI: 10.24425/aee.2019.129350.

[6] Di C., Petrov I., Pyrhönen J.J., Chen J., *Accelerating the Time-Stepping Finite-Element Analysis of Induction Machines in Transient-Magnetic Solutions*, IEEE Access, vol. 7, pp. 122251–122260 (2019), DOI: 10.1109/ACCESS.2019.2938269.

[7] Keränen J., Ponomarev P., Pippuri J., Råback P., Lyly M., Westerlund J., *Parallel performance of multi-slice finite-element modelling of skewed electrical machines*, IEEE Transactions on Magnetics, vol. 53, no. 6, 7201204 (2017), DOI: 10.1109/TMAG.2017.2653421.

[8] Li S., Hofmann H., *Numerically efficient steady-state finite element analysis of magnetically saturated electromechanical devices using a shooting-Newton/GMRES approach*, IEEE Transactions on Magnetics, vol. 39, no. 6, pp. 3481–3485 (2003), DOI: 10.1109/TMAG.2003.819471.

[9] Takahashi Y., Tokumasu T., Kameari A., Kaimori H., Fujita M., Iwashita T., Wakao S., *Convergence acceleration of time-periodic electromagnetic field analysis by the singularity decomposition-explicit error correction method*, IEEE Transactions on Magnetics, vol. 46, no. 8, pp. 2947–2950 (2010), DOI: 10.1109/TMAG.2010.2043721.

[10] Takahashi Y., Tokumasu T., Fujita M., Wakao S., Koji F., Ishihara Y., *Comparison Between Fast Steady-State Analysis Methods for Time-Periodic Nonlinear Magnetic Field Problems*, IEEE Transactions on Magnetics, vol. 48, no. 2, pp. 235–238 (2012), DOI: 10.1109/TMAG.2011.2172579.

[11] Bíró O., Preis K., *An efficient time domain method for nonlinear periodic eddy current problems*, IEEE Transaction on Magnetics, vol. 42, no. 4, pp. 695–698 (2006), DOI: 10.1109/TMAG.2006.871666.

[12] Takahashi Y., Iwashita T., Nakashima H., Tokumasu T., Fujita M., Wakao S., Fujiwara K., Ishihara Y., *Parallel Time-Periodic Finite-Element Method for Steady-State Analysis of Rotating Machines*, IEEE Transaction on Magnetics, vol. 48, no. 2, pp. 1019–1022 (2012), DOI: 10.1109/TMAG.2011.2171923.

[13] von Pfingsten G., Hameyer K., *Highly efficient approach to the simulation of variable-speed induction motor drives*, IET Science, Measurement Technology, vol. 11, no. 6, pp. 793–801 (2017), DOI: https://doi.org/10.1049/iet-smt.2017.0152.

[14] Mertens R., Belmans R., Hamayer K., *Combined Time-Harmonic – Transient Approach to Calculate the Steady-State Behaviour of Induction Machine*, Proceedings of IEEE International Electric Machines and Drives Conference (IEMDC), Seattle, Washington, USA (1999).

[15] Huppunen J., *High-speed solid-rotor induction machine – electromagnetic calculation and design*, PhD Thesis, Helsinki University of Technology, Lappeenranta (2004), DOI: http://lutpub.lut.fi/handle/10024/36551.

[16] Aho T., Nerg J., Pyrhönen J., *Analyzing the effect of the rotor coating on the rotor losses of medium speed solid-rotor induction motor*, Proceedings of International Symposium on Power Electronics, Electrical Drives, Automation and Motion (SPEEDAM 2006), Taormina, Italy, pp. 103–107 (2006), DOI: 10.1109/SPEEDAM.2006.1649752.

[17] Geuzaine C., Remacle J.-F., *Gmsh: a three-dimensional finite element mesh generator with built-in pre- and post-processing facilities*, International Journal for Numerical Methods in Engineering, vol. 79, no. 11, pp. 1309–1331(2009), DOI: https://doi.org/10.1002/nme.2579.

[18] De Gersem H., Hamayer K., *Air-Gap Flux Splitting for the Time-Harmonic Finite-Element Simulation of Single-Phase Induction Machines*, IEEE Transaction on Magnetics, vol. 38, no. 2, pp. 1221–1224 (2002), DOI: 10.1109/20.996312.